SIMS is a very sophisticated technique and utilizes a primary ion beam to produce secondary ions from the surface of the biological sections. SIMS coupled with time of flight (TOF-SIMS) is a superior tool for high-spatial-resolution IMS (submicron order) of elements and small molecules at different organelle levels of the cell [26–28]. However, SIMS lacks the sensitivity for the mass range over m/z 1000, due to in-source fragmentation. DESI allows soft and atmospheric desorption and ionization. DESI has been used in several studies to detect metabolites [29], alkaloids in plant [30], or exogenous and endogenous chemicals in latent fingerprints [31], and it is one of the few ambient ionization methods that have the long-term potential to be translated directly into the operating room to profile tissue during surgery. However, its spatial resolution is inferior to that of other techniques. LAESI is particularly well-suited for the investigation of water-containing specimens. LAESI utilizes a mid-infrared laser beam (2.94-μm wavelength) to excite the water molecules of the sample. A unique aspect of LAESI is depth profiling that, in combination with the lateral imaging, enables three-dimensional (3D) molecular imaging. This instrument is not commercially available now, however. NI-MS is a new surface-based mass spectrometric technique that is well suited for analysis of sterol metabolites [32,33]. Unlike other methods, NI-MS is matrix-free and thereby allows detection of low-mass metabolites without background interference. It is a promising technique that we hope to develop in the future.

MALDI is a soft ionization technique triggered by a pulsed laser beam. The sample is mixed with a matrix or nanoparticles, which absorb light at the wavelength of the laser. MALDI is a very conventional method and the easiest instrument to handle compared with the other developing new techniques. MALDI can ionize biomolecules ranging from small (m/z<1000) [34] to large (m/z>100 kDa) [35]. Due to its wide range of applicability, MALDI-MS is used in various fields, such as proteomics [9,36,37], lipidomics [38–46], metabolomics [47,48], and glycomics [49,50]. The MALDI technique also has some disadvantages in terms of spatial resolution and sensitivity. However, especially in the case of lipid imaging, we consider MALDI the best technique currently available.

2.2. Type of instrument for MALDI-IMS

One requirement for performance of MALDI-IMS is the availability of an x–y moving stage with electronic controls. Most modern MS instruments of the major manufacturers (i.e. Shimadzu, ThermoFisher Scientific, Bruker Daltonics, AB SCIEX, and Waters) can be adapted for MALDI-IMS. TOF is the most widely-used technology. TOF analyzers allow the separation of ionized accelerated molecules according to their mass-to-charge ratio (m/z). TOF-MS offers suitable performance for MALDI-IMS, namely a good transmission ratio (50–100%), sensitivity, and repetition rate. However, TOF-MS lacks the capability to perform effective tandem MS analyses for identification. This disadvantage of TOF-MS has been addressed with the introduction of hybrid analyzers pairing various technologies with TOF: a quadrupole mass analyzer and TOF, a quadrupole ion trap and TOF, an ion mobility spectrometer and TOF, and tandem TOF mass spectrometers. These combination systems have revolutionized the application of TOF-MS to structural analysis with tandem MS analyses. MALDI-IMS is a two-dimensional laser scanning technology. The analyzing time depends on the number of spots, the frequency of the laser, the number of shots per spot, and the time required to moving the stage. The most relevant factor is the frequency of the laser. Almost all of the new MALDI instruments are equipped with 1000-Hz lasers. For example, when users select the region of interest as a 1×1 cm area with a 10-μm scan pitch, there are approximately 10,000 points to be analyzed. Using a 1000-Hz laser with common parameters, this will take only 1 h.

3. Sample preparation for IMS

It is important to optimize the sample preparation procedure according to the characteristic chemical and physical properties of each analyte. The sample preparation procedure needs to be controlled to obtain meaningful images of endogenous molecules in the biological sections. Here, we explain crucial preparation steps for lipid imaging.

3.1. Freezing and sectioning method

This section is devoted to the preparation of tissue sections subjected to MALDI-IMS measurements. The storage of biological tissue samples at −80 °C is required after removal of the target body parts to maintain the integrity and spatial organization of the biomolecules in samples.

Sectioning of thin slices from the tissue samples is another important factor for imaging of the biomolecules' signals. The preferred samples for MALDI-IMS consist of fresh-frozen and chemically unmodified tissue. Fresh-frozen tissues can be prepared using powdered dry ice, liquid nitrogen, liquid nitrogen-chilled isopentane, etc. Among these fresh-freezing methods, the tissue section morphology appears to be well maintained when samples are frozen by powdered dry ice. However, the optimal freezing method is different for different samples. It is important to ensure that the tissue section morphology is well maintained.

Embedding with an optimal cutting temperature (OCT) compound usually allows samples to retain their shape and facilitates the cutting process, but in the preparation of tissue sections for MALDI-IMS measurements, the use of embedding agents such as OCT compound must be avoided because the attachment and penetration of such polymer molecules in tissues cause serious inhibition of biomolecule ionization [51]. Such polymer-like resin compounds generally have high ionization efficiency; this leads to a decrease in the detection sensitivity of other biomolecules. For this reason, when preparing sections for MALDI-IMS, an OCT compound should be used only for "supporting" the tissue blocks so that it does not directly attach to the tissue sections being analyzed. Unfortunately, without this embedding process, difficulties may be encountered in cutting certain tissues into thin sections. In such cases, Stockli et al. used a precooled semiliquid gel of 2% sodium carboxymethylcellulose as an alternative embedding compound that does not interfere with the detection sensitivity of biomolecules by MS analysis [52].

Formaldehyde-fixed and paraffin-embedding (FFPE), the most general preservation condition, could also be used for MALDI-IMS to detect proteins or peptides. Formaldehyde fixation makes IMS analysis difficult because of the protein cross-linking introduced by formaldehyde. The on-tissue proteolytic digestion method, in which proteins are denatured and digested by enzymes, has been developed in order to fix this problem [36,53]. The protocol for this approach was recently published [54]. This method must include a paraffin removal step using xylene and ethanol. FFPE sections were completely stripped of lipids by the deparaffinization step; therefore, it was adapted for detecting proteins or peptides. Lipophilic molecules are also lost during this deparaffinization step; thus, FFPE samples cannot be used for lipid imaging.

Ionization efficiency is partly dependent on the thickness of the tissue section [55]. In general, 5- to 20-μm-thick sections are prepared for the analysis of low-molecular-weight molecules. The use of thinner tissue sections (2–5 μm in thickness) has been recommended for analysis of high-molecular-weight molecules (range, 3–21 kDa) [56]. Sections are thaw-mounted on a stainless steel conductive stage or on commercially available indium-tin oxide (ITO)-coated glass slides. We recommend the use of ITO-coated glass slides because these transparent slides enable microscopic observation of the section after MALDI-IMS. Adhesive film can be used instead of thaw-mounting on the ITO-coated glass slides [57].

Please cite this article as: N. Goto-Inoue, et al., Imaging mass spectrometry for lipidomics, Biochim. Biophys. Acta (2011), doi:10.1016/j.bbalip.2011.03.004

Adhesive film is appropriate for samples for which thaw-mounted preparation of sections is challenging (e.g., rice kernel, bone, or whole-body sections) [58].

3.2. Methods of matrix application

In conventional MALDI-MS analyses, choosing the appropriate matrix is the most important step. General recommendations for each type of biomolecule have been established in traditional MALDI-MS. These recommendations apply also to MALDI-IMS. Generally, 2,5-dihydroxybenzoic acid (DHB) and 9-aminoacridine (9-AA) are used as suitable matrices for lipids and small metabolites [59].

In MALDI-IMS, analytes must be co-crystallized with matrices to be ionized. There are various methods for the coating of the matrix onto the section, such as deposition, spraying, and sublimation. The method of matrix application also influences analyte extraction efficiency. Compared to other methods, the deposition of matrix solution by the use of automatic depositing robotic devices such as a chemical inkjet printer (ChIP-1000; Shimadzu Corporation, Kyoto, Japan) increases the signal sensitivity [60], but decreases the spatial resolution.

Spraying is the most frequently used method in MALDI-IMS [61]. Using this method, an entire tissue section can be coated with relatively small crystals homogeneously in a short time without special equipment. For its operation, several instruments including TLC sprayers and artistic air-brushes are available; we use a metal air-brush with a 0.2-mm nozzle because of its simple and easy-to-handle design. Although this method seems to present few technical challenges, it nonetheless requires skillful operation because of the numerous parameters of the hand-operation of the air-brush. If there is an excess of matrix solution on the tissue, an inhomogeneous crystal can be formed with analytes that have migrated from their original location; on the other hand, if not enough matrix solution is sprayed and it evaporates without sufficiently moisturizing the tissue section, analytes cannot be adequately extracted from the tissue section. The operation should be performed at a constant room temperature and humidity. Beginners are recommended to practice spraying until homogeneous matrix spraying can be achieved reproducibly.

Sublimation is a new method for applying matrix to tissue sections [62]. By using this technique, even an inexperienced researcher could easily apply a uniform coating of matrix over a large sample plate in a very short time (few minutes) without solvents. Additionally, previous reports demonstrated that this method increases the analyte signal and that the fine microcrystals formed from the condensed vapor reduce the limitation of image resolution caused by crystal size [63]. Although it requires a special instrument, we believe that this method will be widespread in the near future.

One of the critical limitations of the spatial resolution of MALDI-IMS is the size of the organic matrix crystal and the analyte migration during the matrix application process. To overcome these problems, other research groups and our group used nanoparticles as new matrices. For example, iron oxide nanoparticles enable the visualization of sulfatide and phospholipid distribution [50,64]; silver nanoparticles can be used for the analysis of fatty acids [65]; and gold nanoparticles are appropriate for the sensitive detection of glycosphingolipids such as sulfatide and ganglioside [66].

3.3. Measurement procedure

MALDI-IMS should be performed as soon as possible after matrix application, regardless of the coating method. To obtain a good spectrum in MALDI-IMS, the procedure is almost the same as that in traditional MALDI-MS; the mass range, detector gain, and laser power must be optimized. From the mechanical setting perspective, there are two differences between MALDI-MS and MALDI-IMS. One difference is that we have to set a two-dimensional region for analyses. In addition, the scan pitch, which decides the spatial resolution of the image, must be fixed because MALDI-IMS can ionize the molecules by laser pulse. The scan pitch, which means the distance between scans, depends on the laser size and mechanical movement control. At this moment, the commercially available instrument with the highest spatial resolution can analyze with a laser diameter of approximately 25 μm [49]. Moreover, we have developed a new instrument, which can move the sample stage by 1 μm, and the finest size of the laser diameter is approximately 10 μm [67]. This instrument achieves the finest images obtainable by MALDI-IMS. MALDI-IMS ionizes numerous compounds on tissue at the same time. Sometimes, we detected plural molecules at the same *m/z* value. In that case, a new imaging technique, "MS/MS imaging", was developed. By the use of this technique, we could separate each ion derived from their specific fragment ions. There are some reports which have shown MS/MS imaging to perform IMS of endogenous metabolites and an exogenous drug [47]. In addition, the combination of ion-mobility separation with MALDI-IMS provides a unique separation dimension to further enhance the capabilities of IMS [68–70]. It can be used to produce images without interference from background ions of similar mass, which can remove ambiguity from imaging experiments and lead to a more precise localization of the compound of interest.

After IMS, further morphological investigations are typically performed. The matrix can be removed by the solvent after IMS. For example, DHB and 9-AA can be removed by methanol. After the completion of MALDI-IMS and matrix removal, tissue samples can be stained by hematoxylin-eosin (HE) to gain further morphological information.

4. Application of MALDI-IMS

MALDI-IMS is currently one of the only methodologies enabling simultaneous visualization of lipids. Visualization of various types of lipids, such as phospholipids [71–76], neutral lipids [77], glycolipids [40,49,78], and fatty acids [65] has been reported. In this section, we introduce the findings of our recent reports on the imaging of lipids.

4.1. MALDI-IMS of phospholipids

Phosphatidylcholines (PCs) are the main constituents of biological membranes, providing an important source for lipid-derived second messengers. Lipid-derived second messengers like inositol phosphates, diacylglycerols, and phosphatidic acids are implicated in the regulation of many cellular functions including proliferation, differentiation, and a number of specific functions [79,80]. Therefore, it is very important to verify the distribution of PCs in biological tissue at the molecular species level. Fig. 1 is an example of imaging of PCs and lysoPC in biological samples, a rat brain and medaka fish (*Oryzias latipes*) [74,76]. We visualized the distribution of ion signals in rat brain tissues which had middle cerebral artery occlusion (MCAO) under deep anesthesia and then decapitated the rat. The ion intensities of PC (diacyl-16:0/18:1) were distributed thoroughly, but exclusively in areas of degeneration in the ipsilateral hemisphere. (Fig. 1a and b). In contrast, the ion distribution of lysoPC (acyl-16:0) was specifically restricted to the area of degeneration in which PC was reduced (Fig. 1c). The merged image (Fig. 1d) shows that PCs and lysoPC were distributed complementarily. These observations raise the possibility that lysoPC might be produced from PCs in the focal ischemic area. Molecular species of lipids can be identified by tandem MS analyses of tissues. A representative tandem MS spectrum of PC (diacyl-16:0/18:1) is shown in Fig. 1e. Neutral loss (NL) of the phosphocholine head group (59 and 183 Da) and fatty acids (256 Da) are usually observed by tandem MS analyses of PC in tissues. Using the MALDI-IMS technique, we could visualize the molecular changes in the injured area following MCAO and identify these molecular species.

The lower panels show the MALDI-IMS results for a medaka fish (*O. latipes*) [76]. PC (diacyl-16:0/18:2) was observed throughout the sections, PC (diacyl-16:0/18:1) was observed to be localized in the brain and liver, while PC (diacyl-16:0/20:4) was intensely detected in the liver (Fig. 1f–h).

Please cite this article as: N. Goto-Inoue, et al., Imaging mass spectrometry for lipidomics, Biochim. Biophys. Acta (2011), doi:10.1016/j.bbalip.2011.03.004

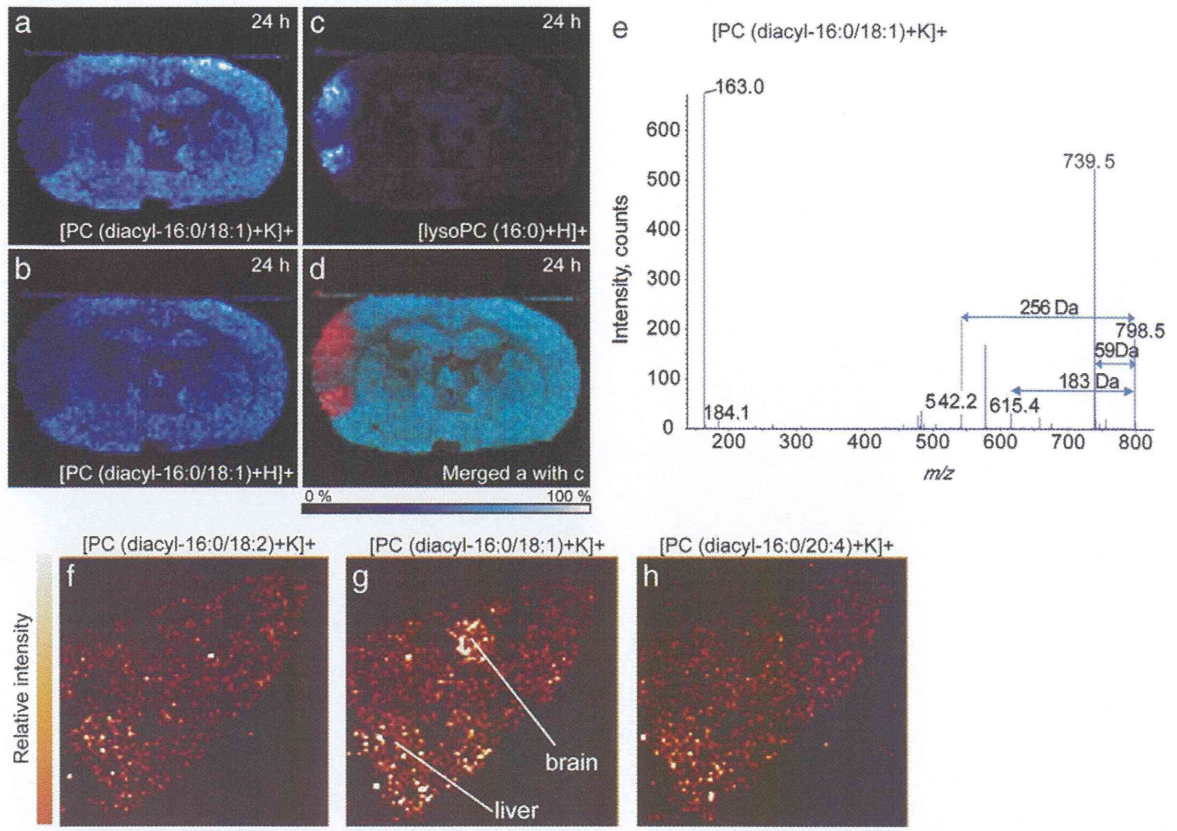

Fig. 1. MALDI-IMS of phospholipids. The upper panel shows the distribution of phospholipids in the rat brain after MCAO. Distributions of $[PC\ (diacyl\text{-}16:0/18:1)+K]^+$ (a), $[PC\ (diacyl\text{-}16:0/18:1)+H]^+$ (b) and $[lysoPC\ (16:0)+H]^+$ (c) in the ischemic brain at 24 h after MCAO as well as a merged image (d) are presented. The ion signals of PCs and lysoPC are indicated by blue and red, respectively. The precursor ion at *m/z* 798.5 was subjected to tandem MS analysis. From the product ions of *m/z* 798.5, NL corresponding to trimethylamine $[N(CH_3)_3$, 59 Da], the cyclophosphane ring ($(CH_2)_2PO_4H$, 124 Da) and the replacement of an adduct ion from potassium to proton (K, 39 Da; H, 1 Da) were observed. The product ion at *m/z* 542.2 corresponding to an NL of a fatty acid (16:0) was also detected (e). The lower panel shows the distribution of PCs in medaka fish (*Oryzias latipes*). (b) Distributions of PC (diacyl-16:0/18:2), PC (diacyl-16:0/18:1), and PC (diacyl-16:0/20:4) are shown (f–h).
Modified, with permission from [74] and [76].

It is hard to visualize metabolites in various kinds of small and minor experimental animals because of the lack of imaging probes. By the use of MALDI-IMS, we could visualize metabolites including lipids without probes. Biomolecules that have a specific distribution might be used as biomarkers to discriminate the geographical origin of animals that have no database of metabolites. This method will be particularly useful in investigating the distribution of lipids in fish since fish oils have beneficial effects on human health.

4.2. MALDI-IMS of neutral lipids

As well as phospholipids, we also performed MALDI-IMS analyses of triacylglycerols (TAGs) with embryo sections. However, there are many kinds of lipids in the mass range of *m/z* 700–1000. Moreover, the distribution of TAGs was constructed from multiple peaks. TAGs have three kinds of fatty acids which make it difficult to speculate the molecular species based on their mass only. Therefore, it is very important to know the fatty acid composition of each TAG. We believed that tandem MS analysis would be preferable for discriminating the different kinds of lipids. Thus, we proved that the identification could be performed by detecting the NLs of fatty acids in the product-ion spectrum for TAG by tandem MS analyses. With embryo sections, we could detect several kinds of molecular species of TAGs. Fig. 2a shows HE staining results from embryo sections. Fig. 2b–d shows the ion images of TAGs (16:1/18:2/18:1), (16:0/20:3/18:1), and (16:0/18:1/18:1). We also show an image merging the three ion images of TAGs with the HE staining (Fig. 2e). It is clear from this image that the TAGs were localized around brown adipose tissue and in the liver. Intriguingly, these signals hardly existed in other areas. Moreover, the merged image of the distribution of the three TAGs (Fig. 2e) highlights the complete correspondence of their distributions. This fascinating localization pattern probably reflects the functional difference of each TAG during embryogenesis, which has not been detected by conventional methods.

4.3. MALDI-IMS of glycolipids

Fig. 3 shows the MALDI-IMS results of glycolipids in testis, or so-called seminolipids. Seminolipids are among the major sulfoglycolipids in mammals [81]. The galactosylation of the sulfoglycolipids is catalyzed by UDPgalactose: ceramide galactosyltransferase (CGT, EC 2.4.1.45) [82]. CGT-deficient mice, which completely lack the ability to produce seminolipids showed an arrest of spermatogenesis, indicating that seminolipids are essential for spermatogenesis [83]. Seminolipids are synthesized in the primary spermatocytes and remain stable during spermatogenesis. It is essential for mammalian development that this process occurs normally [84], although the precise role of seminolipids in spermatogenesis and other processes that take place during and following egg fertilization is still not completely understood. Seminolipids also have some molecular species due to their two kinds of fatty acids. Previous studies demonstrating the distribution of seminolipids have used several antibodies against sulfoglycolipids such as Sulph-1 [85]. However,

Please cite this article as: N. Goto-Inoue, et al., Imaging mass spectrometry for lipidomics, Biochim. Biophys. Acta (2011), doi:10.1016/j.bbalip.2011.03.004

because each of these antibodies recognizes all sulfoglycolipids, including sulfatides, lactosylsulfatides, and seminolipids, none of them is effective for detecting these molecules individually. In addition, it is impossible to identify individual molecular species having different fatty acid chains. To investigate the individual distribution of each molecular species of seminolipids in the testis, we performed MALDI-IMS analyses of the testes at 2 and 8 weeks of age. In mice at the age of 2 weeks, spermatogenesis was still progressing, and the cell stage of the spermatocytes was late pachytene. Mice at the age of 8 weeks had already completed the spermatogenesis process, and all cell types were observed [86]. Direct tissue analyses detected 5 molecular species of seminolipids, *m/z* 767 (C16:0-alkyl-C14:0-acyl or C14:0-alkyl-C16:0-acyl), 795 (C16:0-alkyl-C16:0-acyl), 809 (C17:0-alkyl-C16:0-acyl), 821 (C18:1-alkyl-C16:0-acyl), and 823 (C18:0-alkyl-C16:0-acyl). Fig. 3 shows ion images of the testes at 2 and 8 weeks of age. We observed a major seminolipid, *m/z* 795, throughout the tubules in both the 2- and 8-week-old samples. This result corresponded with previously reported results of the immunostaining of Sulph-1. Next, we investigated the localization of a minor seminolipid, *m/z* 767. We found that *m/z* 767 localized at the edge of tubules, where spermatogonia and spermatocytes exist. The present findings demonstrated that *m/z* 767 is strongly expressed on spermatocytes. Molecules of *m/z* 821 and *m/z* 823 existed throughout the tubules though their peak intensities were low, and the intensities were weaker for the samples from 2-week-old mice than in those from 8-week-old mice. It seems that various seminolipid molecular species appear sequentially according to testicular maturation. On the other hand, *m/z* 809 was expressed in contrast to *m/z* 767. The molecule was expressed in the inner lumen of the tubules of 8-week-old testes and was not clearly detected in 2-week-old testes. In the vicinity of the lumen, spermatids and spermatozoa exist only in 8-week-old testes. Thus, our results indicated that *m/z* 809 was a spermatid- and spermatozoon-specific seminolipid. To identify the detailed localization of molecules which showed cell-specific expression, we tried to overlay these ion images to the optical image of the same section which was stained after MALDI-IMS. We showed that these molecules clearly existed in tubules, and the merged image of *m/z* 767 and 809 demonstrated that these molecules had different distributions. Using the MALDI-IMS technique, we could visualize each molecular species of seminolipid and demonstrate for the first time that each molecular species has a different distribution.

4.4. MALDI-IMS of fatty acids

We also demonstrated a new approach to visualizing fatty acids in mouse retinal samples using silver nanoparticles (AgNPs) as a matrix. The mouse retina is found to be suitable for MALDI-IMS analyses with nanoparticles, possibly due to its complex structure, which includes eight different layers. In the present experiment, mouse retinal sections were analyzed at a high spatial resolution with a scan pitch of 10 μm (gray area in Fig. 4a); then, the ion images corresponding to seven fatty acids were reconstructed (Fig. 4b–h). The ion image of eicosapentaenoic acid (EPA) (20:5) showed the distinct layered structure of the mouse retina. The layers are named as follows: ganglion cell layer (GC), inner plexiform layer (IP), inner nuclear layer (IN), outer plexiform layer (OP), outer nuclear layer (ON), inner segment (IS), outer segment (OS), and pigment epithelium (PEM) from the side of the vitreous body. Our previous study reported that PCs have a three-zonal distribution in mouse retinal sections and that the distributions were divided according to the difference in fatty acid composition in PCs [72]. The ion images reconstructed with the use of

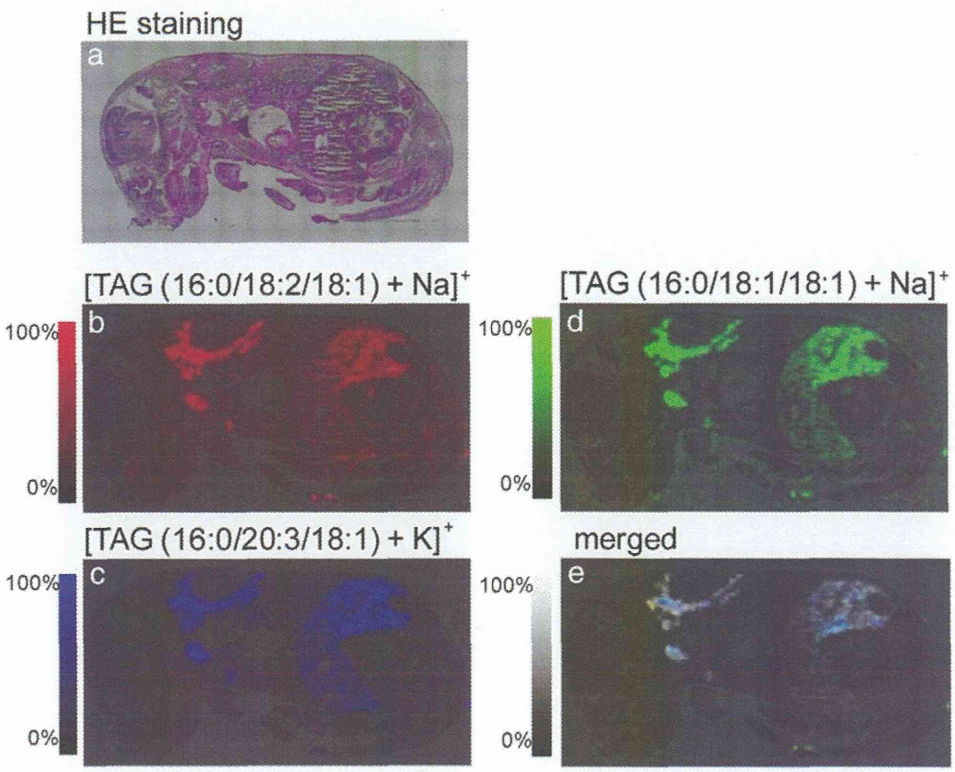

Fig. 2. MALDI-IMS of neutral lipids. Distribution of TAGs in mouse embryo. The HE staining result (a) and ion images of [TAG (16:0/18:2/18:1) + Na]$^+$, [TAG (16:0/18:1/18:1) + Na]$^+$, and [TAG (16:0/20:3/18:1) + K]$^+$ are shown (b–d). The ion images were merged with the optical image of an HE-stained section. The three merged TAG images demonstrate the same distribution.
Modified, with permission from [77].

Please cite this article as: N. Goto-Inoue, et al., Imaging mass spectrometry for lipidomics, Biochim. Biophys. Acta (2011), doi:10.1016/j.bbalip.2011.03.004

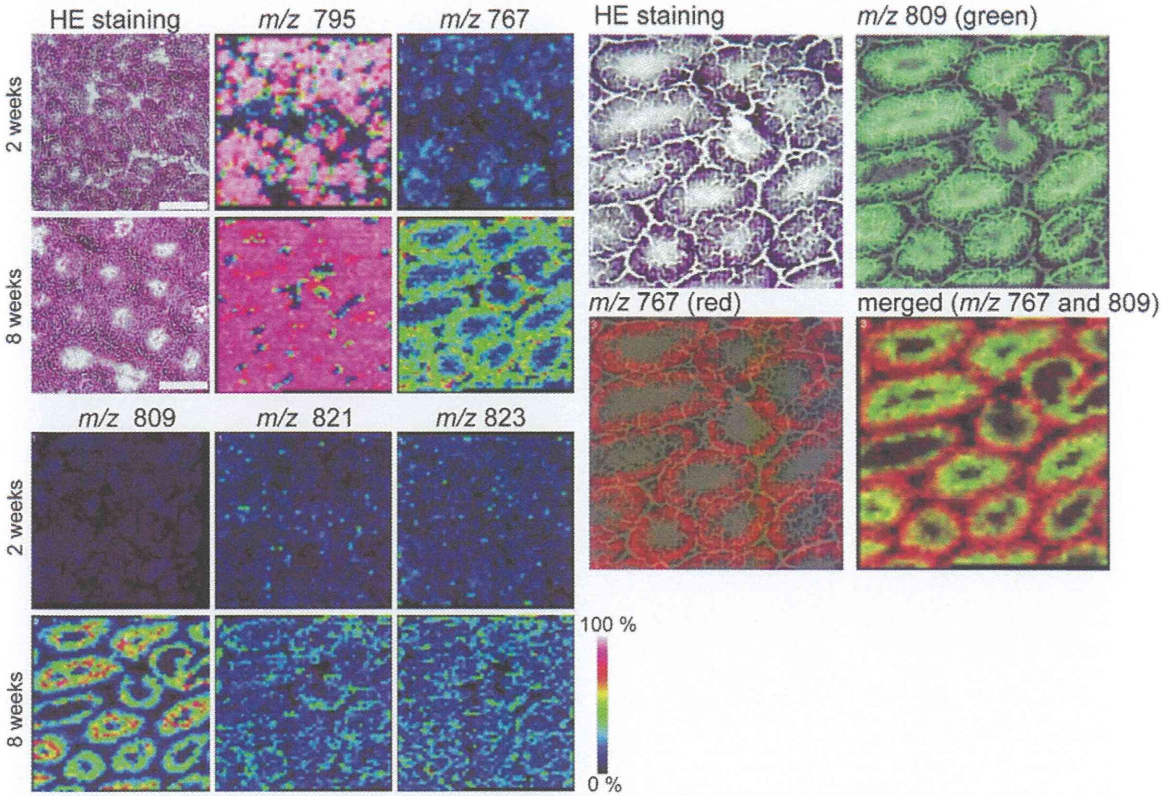

Fig. 3. MALDI-IMS of glycolipids. The optical image of the sample stained with HE staining, and ion images obtained from 2- and 8-week-old mouse testes are shown in the left panel. The optical image of HE staining of the same cryosection which was stained after IMS is also shown in the right panel. The ion images at *m/z* 767 and 809 obtained from 8-week-old mouse testes were merged with the image of HE staining. A merged ion image of *m/z* 767 and 809 is also shown. Bar: 400 μm.
Modified, with permission from [49].

AgNPs showed obviously six-zonal distributions of fatty acids. The ion image showed that palmitic acid (16:0) was distributed in all regions of the mouse retina except the PEM region (Fig. 4b). Linoleic acid (18:2, Fig. 4c), oleic acid (18:1, Fig. 4d), and arachidonic acid (AA; 20:4, Fig. 4g) were equally distributed in the PEM. Stearic acid (18:0) was found in the GC, IP, OP, and PEM regions of the retina (Fig. 4e). However, the ion image of EPA (20:5, Fig. 4f) was similar to the ion image of palmitic acid (Fig. 4b). The ion image of docosahexaenoic acid (DHA) was also slightly apparent at the GC, IP, and OP regions except at the PEM region, where the ion signal was detected at high intensity (Fig. 4h). The present experiment revealed that DHA was concentrated in the PEM in the mouse retina. DHA plays an important role in the development of visual function [87], in promoting survival [88], and in inhibiting apoptosis of photoreceptors [89]. In addition, long-chain poly-unsaturated fatty acids (LCPUFAs) including DHA are a major target of peroxidation, which contributes to several diseases,

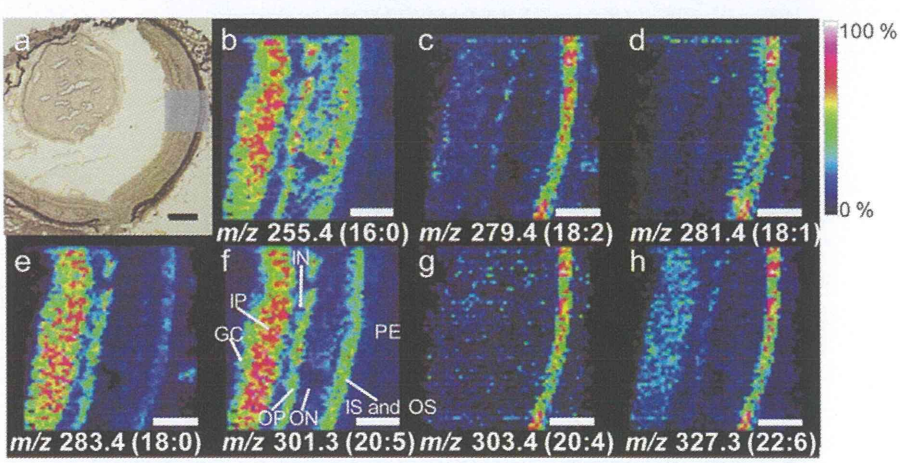

Fig. 4. MALDI-IMS of fatty acids. Visualization of fatty acids in mouse retinal sections with AgNPs. The measurement area is shown by the gray square (a). The ion images were reconstructed from the peaks corresponding to fatty acids, such as palmitic acid (16:0, *m/z* 255.4) (b), linoleic acid (18:2, *m/z* 279.4) (c), oleic acid (18:1, *m/z* 281.4) (d), stearic acid (18:0, *m/z* 283.4) (e), EPA (20:5, *m/z* 301.3), (f), AA (20:4, *m/z* 303.4) (g), and DHA (22:6, *m/z* 327.3) (h). The white scale bars are 100 μm.
Modified, with permission from [65].

Please cite this article as: N. Goto-Inoue, et al., Imaging mass spectrometry for lipidomics, Biochim. Biophys. Acta (2011), doi:10.1016/j.bbalip.2011.03.004

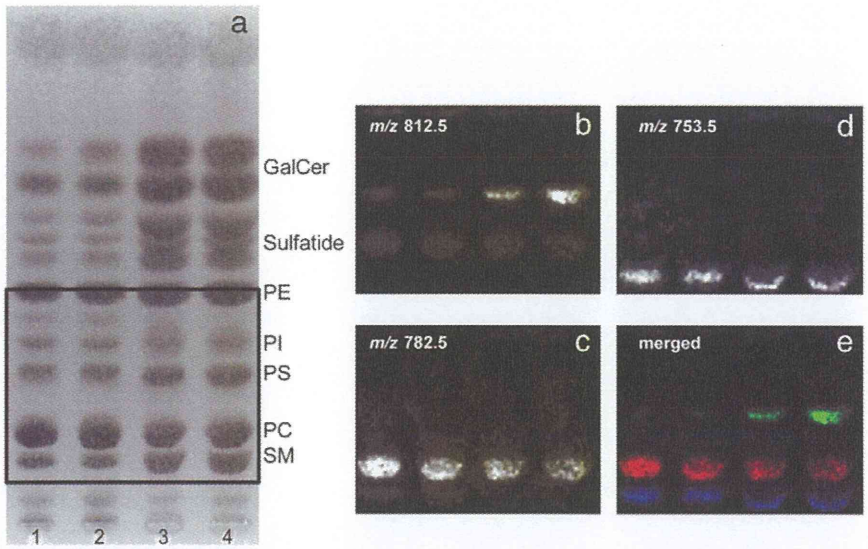

Fig. 5. Application of MALDI-IMS for lipidomics. Thin-layer chromatogram stained with primuline (a). Lanes (1–4) contain human brain lipid extracted from gray matter of the inferior frontal gyrus (lane 1), gray matter of the hippocampus (lane 2), white matter of the inferior frontal gyrus (lane 3), and white matter of the hippocampus (lane 4). The ion images of represented ions at the Rf values of PS, PC, and SM, *m/z* 812.5, 753.5, and 782.5, are shown (b–d). A merged image of these ions (blue; *m/z* 753.5, green; *m/z* 782.5, red; *m/z* 812.5) is also shown (e).
Modified, with permission from [45].

such as age-related macular degeneration [90], diabetic retinopathy [91], and Smith-Lemli-Opitz syndrome [92]. The use of AgNPs in MALDI-IMS might be helpful for learning the distributions of LCPUFAs to elucidate their pathogenesis. Thus, these results indicated that AgNPs were successfully applied to MALDI-IMS analysis of fatty acids in biological samples with heterogeneous structures, such as mouse retinal sections.

5. Application of MALDI-IMS for lipidomics

Although MALDI-IMS is suitable for the analysis of major components in tissue sections, it is difficult to detect minor constituents or molecules that are not easy to ionize because numerous molecules exist in the crude mixture of tissue samples. When crude samples are subjected to MS, numerous molecular species compete for ionization; eventually, molecules that are easily ionized preferentially reach the detector while suppressing the ionization of other molecules [93,94]. Thin-layer chromatography (TLC) is a well-established, inexpensive, and convenient technique for lipid separation [95–97]. However, even under optimized conditions, TLC does not yield unambiguous structural information about individual lipids. We succeeded in highly sensitive detection and detailed structural analysis of lipids using TLC-Blot–MALDI-IMS [41,45,98]. In our methods, lipids on TLC plates were transferred to a polyvinylidene difluoride (PVDF) membrane and the membrane was analyzed by MALDI-IMS. Not only could we analyze the membrane to obtain the relative-to-front (Rf) value of each molecular species, but we could also perform structural analyses by conducting tandem MS analyses. Because the detection limit of lipids depends on MS sensitivity in this case, the sensitivity is expected to be increased compared to the detection using the conventional staining method. We applied this method to total lipids extracted from human brain samples (Fig. 5). By the primuline staining procedure, phosphatidylethanolamine (PE), phosphatidylinositol (PI), phosphatidylserine (PS), PC, and sphingomyelin (SM) were respectively detected as a single, broad band; that is, the lipids were separated depending on the properties of their hydrophilic moieties (Fig. 5a). It is not possible to determine what molecular species are characteristic in each lipid by the chemical staining detection method. In TLC-Blot–MALDI-IMS, however, we can construct individual ion images of their molecular weights, which enable us to visualize each molecular species on a TLC plate and thereby distinguish between the samples. We constructed three ion images at *m/z* 812.5, 782.5, and 753.5. These ions were annotated as PS, PC, and SM based on their Rf values (Fig. 5b–d). A merged image of these ions (blue; *m/z* 753.5, green; *m/z* 782.5, red; *m/z* 812.5) is also shown (Fig. 5e). Based on the molecular mass and Rf value, we could identify these ions as PS (diacyl-18:0/20:4), PC (diacyl-16:0/18:1), and SM (d18:1/C18:0). The molecules at *m/z* 753.5 and 782.5 were somewhat strongly detected in gray matter, but *m/z* 812.5 was detected predominantly in white matter. In the optical image, we could see that all PS and SM molecules were detected strongly in white matter; however, we were able to identify a region-specific distribution of individual lipids in terms of their molecular species by the use of TLC-Blot–MALDI-IMS. This procedure is very easy to conduct; no specific equipment or specific antibodies are required to discriminate and detect analytes. Generally, only one-time TLC, transference to a PVDF membrane, and MALDI-IMS makes it possible to separate, visualize, and identify lipids at a low picomolar level. We believe that this system will be useful in fully analyzing lipid compositions including minor components.

6. Conclusion

MALDI-IMS is becoming an essential tool for molecular imaging of biological samples. MALDI-IMS can facilitate the discovery of characteristic molecules in regions of interest. MALDI-IMS enables us to investigate the localization of known and unknown molecules without labeling, and should facilitate biomarker discovery and validation. Many great advances have already been made with MALDI-IMS in terms of visualizing lipids in various types of biological samples, but there is still room for improvement in sample preparation, ionization, and instrumentation. Moreover, to make the relatively new MALDI-IMS strategy a routine tool for lipidomics, it needs to be validated in larger-scale studies.

Acknowledgments

This work was supported by a Grant-in-Aid for SENTAN from the Japan Science and Technology Agency (to M. S.) and by a Grant-in-Aid for Young Scientists B (to N. G-I.).

References

[1] V.L. Hanson, J.Y. Park, T.W. Osborn, R.M. Kiral, High-performance liquid chromatographic analysis of egg yolk phospholipids, J. Chromatogr. 205 (1981) 393–400.
[2] P.M. Hutchins, R.M. Barkley, R.C. Murphy, Separation of cellular nonpolar neutral lipids by normal-phase chromatography and analysis by electrospray ionization mass spectrometry, J. Lipid Res. 49 (2008) 804–813.
[3] H.Y. Kim, N. Salem Jr., Separation of lipid classes by solid phase extraction, J. Lipid Res. 31 (1990) 2285–2289.
[4] H. Nakanishi, H. Ogiso, R. Taguchi, Qualitative and quantitative analyses of phospholipids by LC–MS for lipidomics, Meth. Mol. Biol. 579 (2009) 287–313.
[5] X. Han, R.W. Gross, Shotgun lipidomics: electrospray ionization mass spectrometric analysis and quantitation of cellular lipidomes directly from crude extracts of biological samples, Mass Spectrom. Rev. 24 (2005) 367–412.
[6] K. Yang, H. Cheng, R.W. Gross, X. Han, Automated lipid identification and quantification by multidimensional mass spectrometry-based shotgun lipidomics, Anal. Chem. 81 (2009) 4356–4368.
[7] H. van Goor, P.O. Gerrits, J. Grond, The application of lipid-soluble stains in plastic-embedded sections, Histochemistry 85 (1986) 251–253.
[8] V.B. Wigglesworth, Histological staining of lipids for the light and electron microscope, Biol. Rev. Camb. Philos. Soc. 63 (1988) 417–431.
[9] F.R. Dani, S. Francese, G. Mastrobuoni, A. Felicioli, B. Caputo, F. Simard, G. Pieraccini, G. Moneti, M. Coluzzi, G. Moneti, A. della Torre, S. Turillazzi, Exploring proteins in *Anopheles gambiae* male and female antennae through MALDI mass spectrometry profiling, PLoS ONE 3 (2008) e2822.
[10] M.L. Pacholski, D.M. Cannon Jr., A.G. Ewing, N. Winograd, Static time-of-flight secondary ion mass spectrometry imaging of freeze-fractured, frozen-hydrated biological membranes, Rapid Commun. Mass Spectrom. 12 (1998) 1232–1235.
[11] N. Bourdos, F. Kollmer, A. Benninghoven, M. Ross, M. Sieber, H.J. Galla, Analysis of lung surfactant model systems with time-of-flight secondary ion mass spectrometry, Biophys. J. 79 (2000) 357–369.
[12] T.P. Roddy, D.M. Cannon Jr., C.A. Meserole, N. Winograd, A.G. Ewing, Imaging of freeze-fractured cells with in situ fluorescence and time-of-flight secondary ion mass spectrometry, Anal. Chem. 74 (2002) 4011–4019.
[13] M.L. Kraft, P.K. Weber, M.L. Longo, I.D. Hutcheon, S.G. Boxer, Phase separation of lipid membranes analyzed with high-resolution secondary ion mass spectrometry, Science 313 (2006) 1948–1951.
[14] N.E. Manicke, J.M. Wiseman, D.R. Ifa, R.G. Cooks, Desorption electrospray ionization (DESI) mass spectrometry and tandem mass spectrometry (MS/MS) of phospholipids and sphingolipids: ionization, adduct formation, and fragmentation, J. Am. Soc. Mass Spectrom. 19 (2008) 531–543.
[15] J.M. Wiseman, D.R. Ifa, A. Venter, R.G. Cooks, Ambient molecular imaging by desorption electrospray ionization mass spectrometry, Nat. Protoc. 3 (2008) 517–524.
[16] A.L. Dill, D.R. Ifa, N.E. Manicke, A.B. Costa, J.A. Ramos-Vara, D.W. Knapp, R.G. Cooks, Lipid profiles of canine invasive transitional cell carcinoma of the urinary bladder and adjacent normal tissue by desorption electrospray ionization imaging mass spectrometry, Anal. Chem. 81 (2009) 8758–8764.
[17] N.E. Manicke, M. Nefliu, C. Wu, J.W. Woods, V. Reiser, R.C. Hendrickson, R.G. Cooks, Imaging of lipids in atheroma by desorption electrospray ionization mass spectrometry, Anal. Chem. 81 (2009) 8702–8707.
[18] M. Girod, Y. Shi, J.X. Cheng, R.G. Cooks, Mapping lipid alterations in traumatically injured rat spinal cord by desorption electrospray ionization imaging mass spectrometry, Anal. Chem. 83 (2011) 207–215.
[19] P. Nemes, A. Vertes, Atmospheric-pressure molecular imaging of biological tissues and biofilms by LAESI mass spectrometry, J. Vis. Exp. 43 (2010).
[20] P. Nemes, A.S. Woods, A. Vertes, Simultaneous imaging of small metabolites and lipids in rat brain tissues at atmospheric pressure by laser ablation electrospray ionization mass spectrometry, Anal. Chem. 82 (2010) 982–988.
[21] G.J. Patti, L.P. Shriver, C.A. Wassif, H.K. Woo, W. Uritboonthai, J. Apon, M. Manchester, F.D. Porter, G. Siuzdak, Nanostructure-initiator mass spectrometry (NIMS) imaging of brain cholesterol metabolites in Smith-Lemli-Opitz syndrome, Neuroscience 170 (2010) 858–864.
[22] G.J. Patti, H.K. Woo, O. Yanes, L. Shriver, D. Thomas, W. Uritboonthai, J.V. Apon, R. Steenwyk, M. Manchester, G. Siuzdak, Detection of carbohydrates and steroids by cation-enhanced nanostructure-initiator mass spectrometry (NIMS) for biofluid analysis and tissue imaging, Anal. Chem. 82 (2010) 121–128.
[23] D.S. Cornett, M.L. Reyzer, P. Chaurand, R.M. Caprioli, MALDI imaging mass spectrometry: molecular snapshots of biochemical systems, Nat. Meth. 4 (2007) 828–833.
[24] S. Shimma, Y. Sugiura, T. Hayasaka, Y. Hoshikawa, T. Noda, M. Setou, MALDI-based imaging mass spectrometry revealed abnormal distribution of phospholipids in colon cancer liver metastasis, J. Chromatogr. B Anal. Technol. Biomed. Life Sci. 855 (2007) 98–103.
[25] Y. Li, B. Shrestha, A. Vertes, Atmospheric pressure infrared MALDI imaging mass spectrometry for plant metabolomics, Anal. Chem. 80 (2008) 407–420.
[26] N.P. Lockyer, Static secondary ion mass spectrometry for biological and biomedical research, Meth. Mol. Biol. 369 (2007) 543–567.
[27] N. Tahallah, A. Brunelle, S. De La Porte, O. Laprevote, Lipid mapping in human dystrophic muscle by cluster-time-of-flight secondary ion mass spectrometry imaging, J. Lipid Res. 49 (2008) 438–454.
[28] H.J. Yang, I. Ishizaki, N. Sanada, N. Zaima, Y. Sugiura, I. Yao, K. Ikegami, M. Setou, Detection of characteristic distributions of phospholipid head groups and fatty acids on neurite surface by time-of-flight secondary ion mass spectrometry, Med. Mol. Morphol. 43 (2010) 158–164.
[29] J.M. Wiseman, D.R. Ifa, Y. Zhu, C.B. Kissinger, N.E. Manicke, P.T. Kissinger, R.G. Cooks, Desorption electrospray ionization mass spectrometry: imaging drugs and metabolites in tissues, Proc. Natl Acad. Sci. U.S.A. 105 (2008) 18120–18125.
[30] Z. Takats, J.M. Wiseman, B. Gologan, R.G. Cooks, Mass spectrometry sampling under ambient conditions with desorption electrospray ionization, Science 306 (2004) 471–473.
[31] D.R. Ifa, N.E. Manicke, A.L. Dill, R.G. Cooks, Latent fingerprint chemical imaging by mass spectrometry, Science 321 (2008) 805.
[32] T.R. Northen, J.C. Lee, L. Hoang, J. Raymond, D.R. Hwang, S.M. Yannone, C.H. Wong, G. Siuzdak, A nanostructure-initiator mass spectrometry-based enzyme activity assay, Proc. Natl Acad. Sci. U.S.A. 105 (2008) 3678–3683.
[33] T.R. Northen, O. Yanes, M.T. Northen, D. Marrinucci, W. Uritboonthai, J. Apon, S.L. Golledge, A. Nordstrom, G. Siuzdak, Clathrate nanostructures for mass spectrometry, Nature 449 (2007) 1033–1036.
[34] A. Svatos, Mass spectrometric imaging of small molecules, Trends Biotechnol. 28 (2010) 425–434.
[35] J.R. Yates III, Mass spectrometry and the age of the proteome, J. Mass Spectrom. 33 (1998) 1–19.
[36] M.R. Groseclose, M. Andersson, W.M. Hardesty, R.M. Caprioli, Identification of proteins directly from tissue: in situ tryptic digestions coupled with imaging mass spectrometry, J. Mass Spectrom. 42 (2007) 254–262.
[37] I. Yao, Y. Sugiura, M. Matsumoto, M. Setou, In situ proteomics with imaging mass spectrometry and principal component analysis in the Scrapper-knockout mouse brain, Proteomics 8 (2008) 3692–3701.
[38] R.C. Murphy, J.A. Hankin, R.M. Barkley, Imaging of lipid species by MALDI mass spectrometry, J. Lipid Res. 50 (Suppl) (2009) S317–S322.
[39] K. Chan, P. Lanthier, X. Liu, J.K. Sandhu, D. Stanimirovic, J. Li, MALDI mass spectrometry imaging of gangliosides in mouse brain using ionic liquid matrix, Anal. Chim. Acta 639 (2009) 57–61.
[40] Y. Sugiura, S. Shimma, Y. Konishi, M.K. Yamada, M. Setou, Imaging mass spectrometry technology and application on ganglioside study; visualization of age-dependent accumulation of C20-ganglioside molecular species in the mouse hippocampus, PLoS ONE 3 (2008) e3232.
[41] N. Goto-Inoue, T. Hayasaka, Y. Sugiura, T. Taki, Y.T. Li, M. Matsumoto, M. Setou, High-sensitivity analysis of glycosphingolipids by matrix-assisted laser desorption/ionization quadrupole ion trap time-of-flight imaging mass spectrometry on transfer membranes, J. Chromatogr. B Anal. Technol. Biomed. Life Sci. 870 (2008) 74–83.
[42] S.N. Jackson, H.Y. Wang, A.S. Woods, M. Ugarov, T. Egan, J.A. Schultz, Direct tissue analysis of phospholipids in rat brain using MALDI-TOFMS and MALDI-ion mobility-TOFMS, J. Am. Soc. Mass Spectrom. 16 (2005) 133–138.
[43] H.Y. Wang, S.N. Jackson, A.S. Woods, Direct MALDI-MS analysis of cardiolipin from rat organs sections, J. Am. Soc. Mass Spectrom. 18 (2007) 567–577.
[44] S.N. Jackson, A.S. Woods, Direct profiling of tissue lipids by MALDI-TOFMS, J. Chromatogr. B Anal. Technol. Biomed. Life Sci. 877 (2009) 2822–2829.
[45] N. Goto-Inoue, T. Hayasaka, T. Taki, T.V. Gonzalez, M. Setou, A new lipidomics approach by thin-layer chromatography–blot-matrix-assisted laser desorption/ionization imaging mass spectrometry for analyzing detailed patterns of phospholipid molecular species, J. Chromatogr. A 1216 (2009) 7096–7101.
[46] N. Zaima, Y. Matsuyama, M. Setou, Principal component analysis of direct matrix-assisted laser desorption/ionization mass spectrometric data related to metabolites of fatty liver, J. Oleo Sci. 58 (2009) 267–273.
[47] Y. Sugiura, M. Setou, Imaging mass spectrometry for visualization of drug and endogenous metabolite distribution: toward in situ pharmacometabolomes, J. Neuroimmune Pharmacol. 5 (2010) 31–43.
[48] M. Burrell, C. Earnshaw, M. Clench, Imaging matrix assisted laser desorption ionization mass spectrometry: a technique to map plant metabolites within tissues at high spatial resolution, J. Exp. Bot. 58 (2007) 757–763.
[49] N. Goto-Inoue, T. Hayasaka, N. Zaima, M. Setou, The specific localization of seminolipid molecular species on mouse testis during testicular maturation revealed by imaging mass spectrometry, Glycobiology 19 (2009) 950–957.
[50] H. Ageta, S. Asai, Y. Sugiura, N. Goto-Inoue, N. Zaima, M. Setou, Layer-specific sulfatide localization in rat hippocampus middle molecular layer is revealed by nanoparticle-assisted laser desorption/ionization imaging mass spectrometry, Med. Mol. Morphol. 42 (2009) 16–23.
[51] S.A. Schwartz, M.L. Reyzer, R.M. Caprioli, Direct tissue analysis using matrix-assisted laser desorption/ionization mass spectrometry: practical aspects of sample preparation, J. Mass Spectrom. 38 (2003) 699–708.
[52] M. Stoeckli, D. Staab, A. Schweitzer, Compound and metabolite distribution measured by MALDI mass spectrometric imaging in whole-body tissue sections, Int. J. Mass Spectrom. 260 (2007) 195–202.
[53] T.C. Rohner, D. Staab, M. Stoeckli, MALDI mass spectrometric imaging of biological tissue sections, Mech. Ageing Dev. 126 (2005) 177–185.
[54] M.C. Djidja, S. Francese, P.M. Loadman, C.W. Sutton, P. Scriven, E. Claude, M.F. Snel, J. Franck, M. Salzet, M.R. Clench, Detergent addition to tryptic digests and ion mobility separation prior to MS/MS improves peptide yield and protein identification for in situ proteomic investigation of frozen and formalin-fixed paraffin-embedded adenocarcinoma tissue sections, Proteomics 9 (2009) 2750–2763.
[55] Y. Sugiura, S. Shimma, M. Setou, Thin sectioning improves the peak intensity and signal-to-noise ratio in direct tissue mass spectrometry, J. Mass Spectrom. Soc. Jpn. 54 (2006) 1–4.
[56] R.J. Goodwin, S.R. Pennington, A.R. Pitt, Protein and peptides in pictures: imaging with MALDI mass spectrometry, Proteomics 8 (2008) 3785–3800.
[57] N. Zaima, N. Goto-Inoue, T. Hayasaka, M. Setou, Application of imaging mass spectrometry for the analysis of *Oryza sativa* rice, Rapid Commun. Mass Spectrom. 24 (2010) 2723–2729.
[58] T. Kawamoto, Use of a new adhesive film for the preparation of multi-purpose fresh-frozen sections from hard tissues, whole-animals, insects and plants, Arch. Histol. Cytol. 66 (2003) 123–143.

Please cite this article as: N. Goto-Inoue, et al., Imaging mass spectrometry for lipidomics, Biochim. Biophys. Acta (2011), doi:10.1016/j.bbalip.2011.03.004

[59] L.A. McDonnell, R.M. Heeren, Imaging mass spectrometry, Mass Spectrom. Rev. 26 (2007) 606–643.
[60] H.R. Aerni, D.S. Cornett, R.M. Caprioli, Automated acoustic matrix deposition for MALDI sample preparation, Anal. Chem. 78 (2006) 827–834.
[61] N.Y. Agar, H.W. Yang, R.S. Carroll, P.M. Black, J.N. Agar, Matrix solution fixation: histology-compatible tissue preparation for MALDI mass spectrometry imaging, Anal. Chem. 79 (2007) 7416–7423.
[62] J.A. Hankin, R.M. Barkley, R.C. Murphy, Sublimation as a method of matrix application for mass spectrometric imaging, J. Am. Soc. Mass Spectrom. 18 (2007) 1646–1652.
[63] V. Vrkoslav, A. Muck, J. Cvacka, A. Svatos, MALDI imaging of neutral cuticular lipids in insects and plants, J. Am. Soc. Mass Spectrom. 21 (2010) 220–231.
[64] S. Taira, Y. Sugiura, S. Moritake, S. Shimma, Y. Ichiyanagi, M. Setou, Nanoparticle-assisted laser desorption/ionization based mass imaging with cellular resolution, Anal. Chem. 80 (2008) 4761–4766.
[65] T. Hayasaka, N. Goto-Inoue, N. Zaima, K. Shrivas, Y. Kashiwagi, M. Yamamoto, M. Nakamoto, M. Setou, Imaging mass spectrometry with silver nanoparticles reveals the distribution of fatty acids in mouse retinal sections, J. Am. Soc. Mass Spectrom. 21 (2010) 1446–1454.
[66] N. Goto-Inoue, T. Hayasaka, N. Zaima, Y. Kashiwagi, M. Yamamoto, M. Nakamoto, M. Setou, The detection of glycosphingolipids in brain tissue sections by imaging mass spectrometry using gold nanoparticles The detection of glycosphingolipids in brain tissue sections by imaging mass spectrometry using gold nanoparticles, J. Am. Soc. Mass Spectrom. 21 (2010) 1940–1943.
[67] T. Harada, A. Yuba-Kubo, Y. Sugiura, N. Zaima, T. Hayasaka, N. Goto-Inoue, M. Wakui, M. Suematsu, K. Takeshita, K. Ogawa, Y. Yoshida, M. Setou, Visualization of volatile substances in different organelles with an atmospheric-pressure mass microscope, Anal. Chem. 81 (2009) 9153–9157.
[68] J. Stauber, L. MacAleese, J. Franck, E. Claude, M. Snel, B.K. Kaletas, I.M. Wiel, M. Wisztorski, I. Fournier, R.M. Heeren, On-tissue protein identification and imaging by MALDI-ion mobility mass spectrometry, J. Am. Soc. Mass Spectrom. 21 (2010) 338–347.
[69] S.N. Jackson, M. Ugarov, T. Egan, J.D. Post, D. Langlais, J. Albert Schultz, A.S. Woods, MALDI-ion mobility-TOFMS imaging of lipids in rat brain tissue, J. Mass Spectrom. 42 (2007) 1093–1098.
[70] J.A. McLean, W.B. Ridenour, R.M. Caprioli, Profiling and imaging of tissues by imaging ion mobility-mass spectrometry, J. Mass Spectrom. 42 (2007) 1099–1105.
[71] T.J. Garrett, M.C. Prieto-Conaway, V. Kovtoun, H. Bui, N. Izgarian, G. Stafford, R.A. Yost, Imaging of small molecules in tissue sections with a new intermediate-pressure MALDI linear ion trap mass spectrometer, Int. J. Mass Spectrom. 260 (2007) 166–176.
[72] T. Hayasaka, N. Goto-Inoue, Y. Sugiura, N. Zaima, H. Nakanishi, K. Ohishi, S. Nakanishi, T. Naito, R. Taguchi, M. Setou, Matrix-assisted laser desorption/ionization quadrupole ion trap time-of-flight (MALDI-QIT-TOF)-based imaging mass spectrometry reveals a layered distribution of phospholipid molecular species in the mouse retina, Rapid Commun. Mass Spectrom. 22 (2008) 3415–3426.
[73] Y. Kobayashi, T. Hayasaka, M. Setou, H. Itoh, N. Kanayama, Comparison of phospholipid molecular species between terminal and stem villi of human term placenta by imaging mass spectrometry, Placenta 31 (2010) 245–248.
[74] S. Koizumi, S. Yamamoto, T. Hayasaka, Y. Konishi, M. Yamaguchi-Okada, N. Goto-Inoue, Y. Sugiura, M. Setou, H. Namba, Imaging mass spectrometry revealed the production of lyso-phosphatidylcholine in the injured ischemic rat brain, Neuroscience 168 (2010) 219–225.
[75] Y. Sugiura, Y. Konishi, N. Zaima, S. Kajihara, H. Nakanishi, R. Taguchi, M. Setou, Visualization of the cell-selective distribution of PUFA-containing phosphatidylcholines in mouse brain by imaging mass spectrometry, J. Lipid Res. 50 (2009) 1776–1788.
[76] N. Zaima, T. Hayasaka, N. Goto-Inoue, M. Setou, Imaging of metabolites by MALDI mass spectrometry, J. Oleo Sci. 58 (2009) 415–419.
[77] T. Hayasaka, N. Goto-Inoue, N. Zaima, Y. Kimura, M. Setou, Organ-specific distributions of lysophosphatidylcholine and triacylglycerol in mouse embryo, Lipids 44 (2009) 837–848.
[78] N. Goto-Inoue, T. Hayasaka, M. Setou, Imaging mass spectrometry of glycolipids, Meth. Enzymol. 478 (2010) 287–301.
[79] K.K. Bhakoo, H.A. Crockard, P.C. Lascelles, S.F. Avery, Prostaglandin synthesis and oedema formation during reperfusion following experimental brain ischaemia in the gerbil, Stroke 15 (1984) 891–895.
[80] J.V. Bonventre, Z. Huang, M.R. Taheri, E. O'Leary, E. Li, M.A. Moskowitz, A. Sapirstein, Reduced fertility and postischaemic brain injury in mice deficient in cytosolic phospholipase A2, Nature 390 (1997) 622–625.
[81] I. Ishizuka, Chemistry and functional distribution of sulfoglycolipids, Prog. Lipid Res. 36 (1997) 245–319.
[82] K. Honke, Y. Hirahara, J. Dupree, K. Suzuki, B. Popko, K. Fukushima, J. Fukushima, T. Nagasawa, N. Yoshida, Y. Wada, N. Taniguchi, Paranodal junction formation and spermatogenesis require sulfoglycolipids, Proc. Natl Acad. Sci. U.S.A. 99 (2002) 4227–4232.
[83] T. Coetzee, N. Fujita, J. Dupree, R. Shi, A. Blight, K. Suzuki, B. Popko, Myelination in the absence of galactocerebroside and sulfatide: normal structure with abnormal function and regional instability, Cell 86 (1996) 209–219.
[84] H. Fujimoto, K. Tadano-Aritomi, A. Tokumasu, K. Ito, T. Hikita, K. Suzuki, I. Ishizuka, Requirement of seminolipid in spermatogenesis revealed by UDP-galactose: ceramide galactosyltransferase-deficient mice, J. Biol. Chem. 275 (2000) 22623–22626.
[85] Y.L. Zhang, Y. Hayashi, X.Y. Cheng, T. Watanabe, X.C. Wang, N. Taniguchi, K. Honke, Testis-specific sulfoglycolipid, seminolipid, is essential for germ cell function in spermatogenesis, Glycobiology 15 (2005) 649–654.
[86] K. Tadano-Aritomi, J. Matsuda, H. Fujimoto, K. Suzuki, I. Ishizuka, Seminolipid and its precursor/degradative product, galactosylalkylacylglycerol, in the testis of saposin A- and prosaposin-deficient mice, J. Lipid Res. 44 (2003) 1737–1743.
[87] J.M. Alessandri, B. Goustard, P. Guesnet, G. Durand, Docosahexaenoic acid concentrations in retinal phospholipids of piglets fed an infant formula enriched with long-chain polyunsaturated fatty acids: effects of egg phospholipids and fish oils with different ratios of eicosapentaenoic acid to docosahexaenoic acid, Am. J. Clin. Nutr. 67 (1998) 377–385.
[88] N.P. Rotstein, M.I. Aveldano, F.J. Barrantes, L.E. Politi, Docosahexaenoic acid is required for the survival of rat retinal photoreceptors in vitro, J. Neurochem. 66 (1996) 1851–1859.
[89] N.P. Rotstein, M.I. Aveldano, F.J. Barrantes, A.M. Roccamo, L.E. Politi, Apoptosis of retinal photoreceptors during development in vitro: protective effect of docosahexaenoic acid, J. Neurochem. 69 (1997) 504–513.
[90] M. Suzuki, M. Kamei, H. Itabe, K. Yoneda, H. Bando, N. Kume, Y. Tano, Oxidized phospholipids in the macula increase with age and in eyes with age-related macular degeneration, Mol. Vis. 13 (2007) 772–778.
[91] H.Z. Pan, H. Zhang, D. Chang, H. Li, H. Sui, The change of oxidative stress products in diabetes mellitus and diabetic retinopathy, Br. J. Ophthalmol. 92 (2008) 548–551.
[92] D.A. Ford, J.K. Monda, R.S. Brush, R.E. Anderson, M.J. Richards, S.J. Fliesler, Lipidomic analysis of the retina in a rat model of Smith-Lemli-Opitz syndrome: alterations in docosahexaenoic acid content of phospholipid molecular species, J. Neurochem. 105 (2008) 1032–1047.
[93] T.M. Annesley, Ion suppression in mass spectrometry, Clin. Chem. 49 (2003) 1041–1044.
[94] G.P. Gellermann, T.R. Appel, P. Davies, S. Diekmann, Paired helical filaments contain small amounts of cholesterol, phosphatidylcholine and sphingolipids, Biol. Chem. 387 (2006) 1267–1274.
[95] K. Korte, M.L. Casey, Phospholipid and neutral lipid separation by one-dimensional thin-layer chromatography, J. Chromatogr. 232 (1982) 47–53.
[96] S. Rodriguez, M.V. Cesio, H. Heinzen, P. Moyna, Determination of the phospholipid/lipophilic compounds ratio in liposomes by thin-layer chromatography scanning densitometry, Lipids 35 (2000) 1033–1036.
[97] A.M. Weerheim, A.M. Kolb, A. Sturk, R. Nieuwland, Phospholipid composition of cell-derived microparticles determined by one-dimensional high-performance thin-layer chromatography, Anal. Biochem. 302 (2002) 191–198.
[98] N. Zaima, N. Goto-Inoue, T. Hayasaka, M. Setou, Selective analysis of lipids by thin-layer chromatography blot matrix-assisted laser desorption/ionization imaging mass spectrometry, J. Oleo Sci. 60 (2011) 93–98.

Please cite this article as: N. Goto-Inoue, et al., Imaging mass spectrometry for lipidomics, Biochim. Biophys. Acta (2011), doi:10.1016/j.bbalip.2011.03.004

第64巻第6号 2013年12月15日発行(年6回2・4・6・8・10・12月の15日発行) 1999年3月1日第三種郵便物認可
ISSN 0370-9531 Seitai no Kagaku

生体の科学

SEITAI NO KAGAKU

Vol.64 No.6 2013 Nov.-Dec.

[特集]顕微鏡で物を見ることの新しい動き

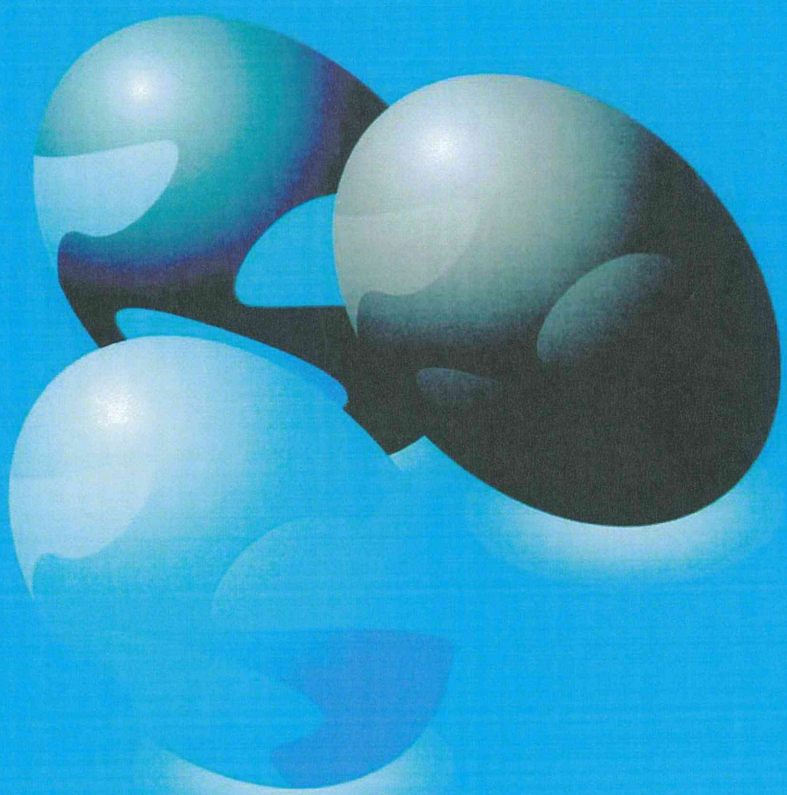

公益財団法人金原一郎記念医学医療振興財団／医学書院

生体の科学　64(6):614-620, 2013

特集　顕微鏡で物を見ることの新しい動き

質量顕微鏡法を用いた生体組織解析

佐野圭吾　瀬藤光利

質量顕微鏡は物質の同定や構造決定に力を発揮する質量分析法と，微細構造解析を行う顕微鏡法を融合させた解析装置である。質量分析によって得られる生化学的情報と位置情報を組み合わせることにより，検出された質量ごとの分布を可視化する質量イメージングを行うことが可能であり，質量イメージング装置の中でイメージングの解像度が肉眼解像度(100 μm)を上回るものを特に質量顕微鏡と言う。質量顕微鏡は物質の質量を直接検出するので抗体やプローブなどによる標識を必要としない。このため対象物質を限定することなく，未知の物質も含めた数千に及ぶ生体分子の検出・同定が可能である。この特徴は，これまで見ることのできなかった脂質や低分子化合物の生体内分布についての新たな知見をもたらしている。本稿では質量顕微鏡の原理について説明すると共に，質量顕微鏡によって得られた生体組織解析の知見や今後の展望について紹介する。

質量顕微鏡のための質量分析法

光学観察を行い試料のイオン化を行うイオン化部と，質量分析のための装置からなる質量分析部によって構成される(図1)。質量分析法は原子，分子，クラスターなどの粒子をイオン化させ，それらのイオンの質量電荷比(質量/電荷：m/z)に応じて分離・検出し，分子量を分析する手法である。質量分析法におけるイオン化法は様々な手法が用いられている[1]。

質量顕微鏡で最も一般的なイオン化法はマトリックス支援レーザー脱離イオン化(matrix assisted Laser desorption/ionization：MALDI)である。MALDIは2002年にノーベル化学賞を受賞された田中ら[2]と，Hillenkamp，Karasら[3]によって開発された。解析物質を結晶マトリックスによって包み込み，そこにパルスレーザー照射することによって物質をイオン化する方法である。レーザー照射による熱エネルギーがマトリックスに吸収されるため，従来のイオン化法では壊れやすかった分子量10万以上のタンパク質やDNAなどの高分子生体物質の分析が可能となった。MALDIでは解析対象物質に適したマトリックスを選択し，そのマトリックスと試料が緊密に混ざり合って結晶化され，解析対象物質のイオン化が行われやすくなっていることが必要である。さらに質量顕微鏡では解析対象物質の組織内分布を崩さずに塗布することが可能な化合物でなければない。

MALDI以外を用いた質量顕微鏡には二次イオン質量分析(secondary ion mass spectrometry：SIMS)が古くから開発されてきた。SIMSはLieblとHerzogによってアメリカ航空宇宙局(NASA)の補助を受けて1960年代に装置として完成され[4]，試料の表面にビーム状のイオン(一次イオン)を照射し，そのイオンと試料表面の分子・

Analysis of physiological tissue with mass microscopy
Sano Keigo, Setou Mitsutoshi：浜松医科大学医学部 解剖学講座 細胞生物学分野(〒431-3192 静岡県浜松市東区半田山1-20-1)

0370-9531/12/¥500/論文/JCOPY